Direction reversal of non-Hermitian skin effect via coherent coupling

Linhu Li [1,*] Wei Xin Teo [2] Sen Mu,[2,†] and Jiangbin Gong[2,3,‡]

[1]*Guangdong Provincial Key Laboratory of Quantum Metrology and Sensing & School of Physics and Astronomy, Sun Yat-Sen University (Zhuhai Campus), Zhuhai 519082, China*

[2]*Department of Physics, National University of Singapore, Singapore 117551, Singapore*

[3]*Centre for Quantum Technologies, National University of Singapore, Singapore 117543, Singapore*

Absolute negative mobility (ANM) in nonequilibrium systems depicts the possibility of particles propagating toward the opposite direction of an external force. We uncover in this work a phenomenon analogous to ANM regarding eigenstate localization and particle transport in non-Hermitian systems under the influence of the non-Hermitian skin effect (NHSE). A coherent coupling between two non-Hermitian chains individually possessing the same preferred direction of NHSE is shown to cause a direction reversal of NHSE for all eigenmodes. This concept is further investigated in terms of time evolution dynamics using a non-Hermitian quantum walk platform within reach of current experiments. Our findings are explained both qualitatively and quantitatively. The possible direction reversal of NHSE can potentially lead to interesting applications.

Introduction. Non-Hermitian Hamiltonians provide an effective description of open quantum systems or wave systems with gain and loss [1–5]. One main feature of non-Hermitian lattice systems with nonreciprocity is the seminal non-Hermitian skin effect (NHSE) under open boundary conditions [6,7]. NHSE causes directional accumulation of eigenmodes at the system's boundaries and has a rather deep connection with the point-gap topology of the complex spectrum of non-Hermitian systems [6–20]. NHSE has spurred considerable interest in condensed matter physics research because it challenged our conventional thinking of bulk-edge correspondence [21–23] and has motivated the so-called non-Bloch band theory [7,9,10]. Much attention has also been paid to the interplay between the NHSE and other important physical effects, such as external electromagnetic fields [24–26], disorders and defects [27–35], and its hybridization [15,16,36–38] or competition [39–41] with topological localization.

Nonreciprocal hopping on a one-dimensional (1D) lattice defines a preferred direction analogous to a physical direction of an external force. The preferred boundary for bulk state localization as NHSE is thus intuitive, so does the preferred direction favoring particle transport [11,16,19,42–46]. For example, if the strength of intercell hopping to the left is always larger than that to the right, then NHSE is expected to localize all states at the left boundary. On the other hand, we must take note of one remarkable dynamical phenomenon in systems far from equilibrium, namely, absolute negative mobility (ANM), where particles propagate toward the opposite direction of an external force [47–59]. Recognizing non-Hermitian systems as nonequilibrium systems, it is necessary to address the possibility of population accumulation or particle transport in a direction against the preferred direction indicated by the nonreciprocal hopping. This issue is not only of theoretical interest, but may offer versatile control knobs to manipulate NHSE for various applications, such as light funneling [60] and directional signal amplification [42,43,61].

In this work, we unveil a general scheme to induce 1D NHSE in a direction precisely opposite to the favored direction of nonreciprocal hopping, as sketched in Fig. 1. As shown below, this exotic phenomenon can be obtained at both the eigenstate level and the dynamics level. There can be multiple interpretations of why a direction reversal of NHSE occurs. Among them, a simple physical picture adopted below is based on the interference between multiple hopping pathways. Specifically, if two non-Hermitian lattices with the same preferred nonreciprocal direction are coupled, then multiple hopping pathways become available. The resulting interference between the multiple hopping pathways can counterintuitively and drastically alter the effective strengths of hopping towards two directions and hence one must reexamine the true physically favored direction of NHSE.

The direction reversal of NHSE by coherent coupling is in principle observable in a variety of quantum and classical platforms realizing NHSE [44–46,60,62–67]. In particular, reversed NHSE at the eigenstate level is already within the reach of classical platforms, such as circuits. However, how reversed NHSE is manifested at the dynamics level is less straightforward. We hence propose a nonunitary quantum walk setting directly addressing non-Hermitian dynamics [44–46], with the essential addition being an interchain hopping for the quantum walker along two chains. As elaborated below, even though the preferred direction of NHSE is no longer obvious in the quantum walk dynamics, the multiple propagation

*lilh56@mail.sysu.edu.cn
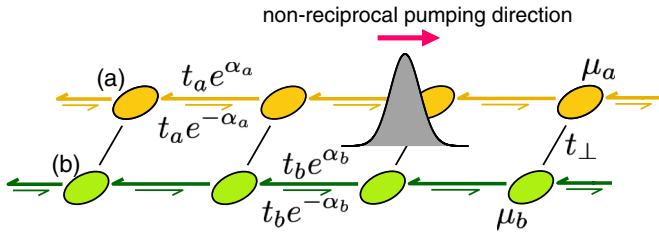†senmu@u.nus.edu
‡phygj@nus.edu.sg

FIG. 1. Schematic of two coupled chains with nonreciprocal hoppings. In either lattice, the amplitude of hopping to the left direction is $t_s e^{\alpha_s}$ ($s = a, b$), apparently with a magnitude larger than that to the right direction $t_s e^{-\alpha_s}$. $t_\perp$ introduces coupling between the two chains and hence multiple hopping pathways from one lattice site to its neighboring site.

pathways induced by the interchain hopping can still lead to a direction reversal of particle transport.

Direction reversal of eigenstate population accumulation. Our starting point is a minimal model depicting two coupled non-Hermitian chains [68] with different on-site potentials, as shown in Fig. 1. The real-space Hamiltonian reads

$$\hat{H} = \sum_{x=1}^{L} \sum_{s=a,b} [t_s e^{\alpha_s} \hat{s}_x^\dagger \hat{s}_{x+1} + t_s e^{-\alpha_s} \hat{s}_x^\dagger \hat{s}_{x-1}$$
$$+ t_\perp (\hat{a}_x^\dagger \hat{b}_x + \hat{b}_x^\dagger \hat{a}_x) + \mu_a \hat{a}_x^\dagger \hat{a}_x + \mu_b \hat{b}_x^\dagger \hat{b}_x,], \quad (1)$$

with t_s and $\alpha_s > 0$ determining the asymmetric hopping amplitudes on the two chains labeled by $s = a, b$. Referring to Fig. 1, the preferred direction of the nonreciprocal hopping here is apparently to the left for both chains. The on-site potential is set to be $\mu_a = -\mu_b = \mu$, with all other choices being equivalent upon shifting their eigenenergies. The two chains are completely decoupled if $t_\perp = 0$, each displaying NHSE localization at the left edge, with an inverse localization length $\kappa_{a,b} = \alpha_{a,b}$ [7,10,15]. An example depicting such a decoupling limit is illustrated in Fig. 2(a).

Upon switching on the interchain coupling ($t_\perp \neq 0$), both the complex spectrum and eigenstate localization of the coupled system start to differ from that of the uncoupled case, no matter how small $t_\perp$ is [17,69,70]. To allow for many hopping pathways from one site to its neighboring site, such as $a_x \to a_{x+1}$ and $a_x \to b_x \to b_{x+1} \to a_{x+1}$, to interfere significantly, here we investigate a strong coupling regime with sufficiently large $t_\perp$. It is then found that *all* eigenmodes can now localize at the opposite edge as compared with that in the uncoupled case. This is clearly seen in Figs. 2(a)–2(c) as the interchain coupling strength $t_\perp$ increases from 0 to 6 and to 15.

To characterize the above-observed direction reversal of NHSE, we consider averages of the standard and directional inverse participation ratios (IPR and dIPR), defined as

$$\bar{I} = \frac{1}{2L} \sum_m \sum_{x=1}^{L} (|\psi_{x,m}^a|^4 + |\psi_{x,m}^b|^4), \quad (2)$$

$$\bar{I}_d = \frac{1}{2L} \sum_m \sum_{x=1}^{L} \frac{[x - (L+1)/2](|\psi_{x,m}^a|^4 + |\psi_{x,m}^b|^4)}{(L-1)/2}, \quad (3)$$

with $\psi_{x,m}^s$ the wave amplitude of the mth normalized right eigenmode at site x of sublattice s. Representative results are
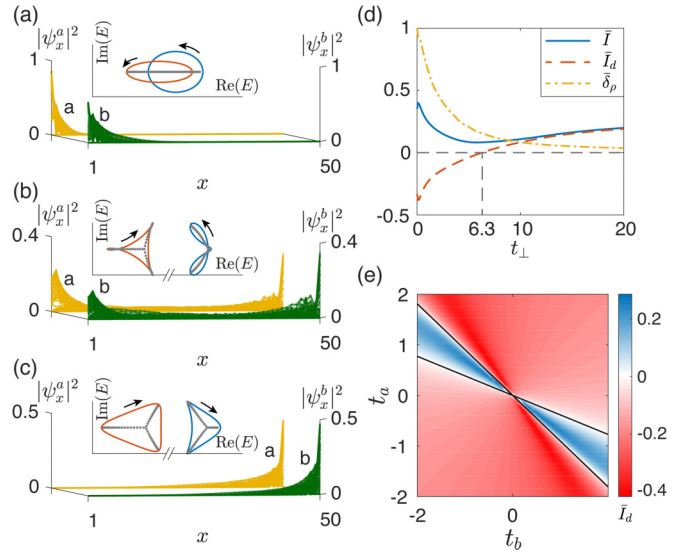

FIG. 2. (a)–(c) Distribution of all eigenmodes on the two chains, with different interchain coupling $t_\perp = 0, 6, 15$, respectively. Insets show the corresponding spectra under PBC (red and blue for the two bands) and OBC (gray). Clockwise and counterclockwise winding directions of the PBC spectra versus the quasimomentum k, as indicated by the black arrows, correspond to OBC skin modes localized on the left and right, respectively [12–14]. Note that, in (b) and (c), we have omitted a large spacing in Re[E] between the two energy bands (red and blue), represented by the double slash in the axis. Other parameters are $t_a = 0.75$, $t_b = -1$, $\alpha_a = 0.5$, $\alpha_b = 0.2$, and $\mu_a = -\mu_b = 0.5$. (d) $\bar{I}$, $\bar{I}_d$, and $\bar{\delta}_\rho$ defined in Eqs. (2), (3), and (4) versus the interchain coupling $t_\perp$, with the same parameters as in (a)–(c). (e) Phase diagram regarding the directional IPR $\bar{I}_d$ at $t_\perp = 30$ with other parameters the same as (a)–(c). Black lines are obtained from the perturbation results of Eq. (8).

presented in Fig. 2(d). It is seen that the IPR (and the absolute value of dIPR) gets larger either for weaker or stronger $t_\perp$, indicating a stronger boundary accumulation of the eigenmodes, but with opposite accumulating directions, as evidenced by the signs of the dIPR. A reversal of the NHSE direction starts to occur when $\bar{I}_d = 0$, which is at $t_\perp \approx 6.3$ in the shown example. In the neighborhood of the transition point $\bar{I}_d = 0$ (see Fig. 2), the eigenmodes can possibly localize at both boundaries in a balanced manner as the bipolar NHSE [66,71]. More importantly, away from the transition point, *all* eigenmodes are now localized at the opposite boundary as compared with the uncoupled case. Meanwhile, the difference between the average distribution on the two lattices, defined as

$$\bar{\delta}_\rho = \frac{1}{2L} \sum_m \left| \sum_{x=1}^{L} (|\psi_{x,m}^a|^2 - |\psi_{x,m}^b|^2) \right|, \quad (4)$$

is seen to decrease with increasing $t_\perp$, indicating a stronger hybridization between the two chains at larger $t_\perp$. We note that the NHSE and its direction reversal are protected by a point-gap topology characterized by the spectral winding number [13,14] and are thus robust to disorder [72].

Physics of reversed NHSE. To confirm that the main physics behind reversed NHSE is the interference between multiple hopping pathways, we consider a straightforward first-order

perturbation theory by treating $\hat{H}_\perp = t_\perp \sum_x (\hat{a}_x^\dagger \hat{b}_x + \hat{b}_x^\dagger \hat{a}_x)$ as the unperturbed Hamiltonian. The unperturbed eigenmodes at site x are simply given by local hybridized adiabatic modes of the coupled system, i.e.,

$$|u_{\pm,x}\rangle = \hat{u}_{\pm,x}^\dagger |0\rangle = (\hat{a}_x^\dagger \pm \hat{b}_x^\dagger)|0\rangle/\sqrt{2}, \quad E_{\pm,x} = \pm t_\perp, \quad (5)$$

with $|0\rangle$ the vacuum and $E_{\pm,x}$ the corresponding unperturbed eigenenergies due to the coherent coupling. By taking all the rest terms as a perturbation, we rewrite the nonreciprocal hopping Hamiltonian in the local adiabatic representation, yielding

$$\hat{H}_\pm' = \sum_x (t_a e^{\alpha_a} + t_b e^{\alpha_b})\hat{u}_{\pm,x}^\dagger \hat{u}_{\pm,x+1} + (t_a e^{-\alpha_a} + t_b e^{-\alpha_b})$$
$$\times \hat{u}_{\pm,x+1}^\dagger \hat{u}_{\pm,x} + (\mu_a \pm \mu_b)\hat{u}_{\pm,x}^\dagger \hat{u}_{\pm,x}. \quad (6)$$

Interestingly, other than the local on-site energy being expectedly different, the "+" and "−" hybridized lattice sites have the same nonreciprocal hopping strengths—$(t_a e^{\alpha_a} + t_b e^{\alpha_b})$ to the left and $(t_a e^{-\alpha_a} + t_b e^{-\alpha_b})$ to the right. That is, the effective hopping amplitudes are seen to be a sum of two individual hopping amplitudes $t_a e^{\alpha_a}$ and $t_b e^{\alpha_b}$ or $t_a e^{-\alpha_a}$ and $t_b e^{-\alpha_b}$, thus clearly indicating an interference mechanism. Most importantly, if t_a and t_b are of different signs, then there is a destructive interference between the two favored amplitudes. This can then lead to

$$|t_a e^{-\alpha_a} + t_b e^{-\alpha_b}| > |t_a e^{\alpha_a} + t_b e^{\alpha_b}|, \quad (7)$$

meaning that NHSE here should accumulate/localize population to the right for *all* the eigenmodes, opposite to the NHSE direction on the uncoupled chains. Inequality (7) also suggests that reversed NHSE occurs within the following parameter regime:

$$\frac{t_a}{-t_b} \in \left(\frac{e^{\alpha_b} - e^{-\alpha_b}}{e^{\alpha_a} - e^{-\alpha_a}}, \frac{e^{\alpha_b} + e^{-\alpha_b}}{e^{\alpha_a} + e^{-\alpha_a}} \right), \quad (8)$$

as shown by the solid lines in Fig. 2(e). The transition lines obtained this way match well with the numerical results based on the sign of the average directional IPR $\bar{I}_d$. A momentum space perturbation theory together with the so-called generalized Brillouin zone [7,9] yields the same prediction in theory, as detailed in the Supplemental Material [72]. Note also that the role of the on-site potential difference μ is not seen here due to our first-order treatment or the strong coupling assumption. The actual threshold value $t_\perp$ to enter the reversed NHSE regime gradually increases with μ.

As elaborated above, the destructive interference between the two chains requires hopping amplitudes along them to have different signs, which is nontrivial, but implementable in various experimental platforms realizing the NHSE. For example, effective couplings with opposite signs can be generated by inductors and capacitors in RLC circuit lattices as a result of their opposite quarter-period phase shifts [74], or by linking acoustic cavities with different connectivity according to the field morphologies of resonators in acoustic lattices [75]. Noticing that negative couplings here can be associated with an effective π flux within each unit cell, it is convenient to exploit a gauge transformation $\hat{b}_x^\dagger \to (-1)^{x-1}\hat{b}_x^\dagger$, so as to avoid possible experimental

difficulty to have negative values and non-Hermiticity simultaneously [72]. On the other hand, reversed NHSE may also be obtained under $t_a t_b > 0$, if we introduce multiple hopping pathways in other manners, such as allowing for off-diagonal couplings between the two chains. These details can be found in the Supplemental Material [72].

Reversed particle transport in non-Hermitian quantum walk. So far, the reversed NHSE is investigated on the eigenstate level via population accumulation against the preferred direction of nonreciprocal hopping. To make a closer analogy to ANM, it is necessary to explore how this leads to particle transport along a reversed direction. To motivate experimental interest, we use an available and fruitful platform, namely, a discrete-time nonunitary quantum walk model realizing the NHSE through single-photon dynamics in a 1D chain [44–46]. We now propose a quantum walker along two chains, plus a local interchain exchange depending on the spin state. Such a structure allows different propagation pathways to acquire different phases from the Floquet dynamics itself, thus avoiding the prerequisite to engineer a negative coupling on the lattice.

Specifically, we consider the following two Floquet operators governing the quantum walk:

$$U_0 = R(\theta_1)S_2 R(\theta_2 + \theta_3)MR(\theta_2 + \theta_3)S_1 R(\theta_1), \quad (9)$$

$$U = R(\theta_1)S_2 R(\theta_2)S_4 R(\theta_3)MR(\theta_3)S_3 R(\theta_2)S_1 R(\theta_1). \quad (10)$$

Here $R(\theta)$ rotates the spin by θ about the y axis, with $R(\theta) = \sum_{x=-N}^{N} \sum_{s=a,b} |s,x\rangle\langle s,x| \otimes e^{-i\lambda_s \theta \sigma_y/2}$, $s = a, b$ denoting the two chains, x the site index, and $\lambda_a = 1$ and $\lambda_b = -1$. The shift operators S_1 and S_2 are standard quantum walk operations, as they shift the walker to the left and right along either chain, if and only if the spin is up and down, respectively. Nonunitarity/non-Hermiticity is introduced through the operator M, with

$$M = \sum_{x=-N}^{N} \sum_{s=a,b} |s,x\rangle\langle s,x| \otimes (|\downarrow\rangle\langle\downarrow| + e^{-\alpha_s}|\uparrow\rangle\langle\uparrow|)$$

describing the (quasi)particle loss only for the spin-up component. U_0 thus defined above yields exactly two copies of the quantum walk model realizing the NHSE in Refs. [44–46], but with opposite spin rotation angles through the parameter λ_s. The M operator alone seems to suggest that the spin-down channel is favored. This effect further interplays with the spin rotation operator $R(\theta)$ and the shift operators $S_{1,2}$ to yield nonreciprocal particle transport, with the preferred direction no longer obvious. Despite the difference in λ_s between the two quantum walk copies, their preferred direction of transport is found to be always the same.

We now couple the two chains accommodating U_0, thus defining our quantum walk model U. U is obtained by inserting S_3 and S_4 into U_0. S_3 and S_4 are almost the same operations as S_1 and S_2 except that the walker is instructed to hop onto the other chain (of the same lattice index) when the spin state is up and down, respectively. Detailed definitions of these operations are shown in the Supplemental Material [72]. S_3 and S_4 are expected to hybridize the two chains and induce interference between multiple hopping pathways. We aim to show that even though the two individual chains have the
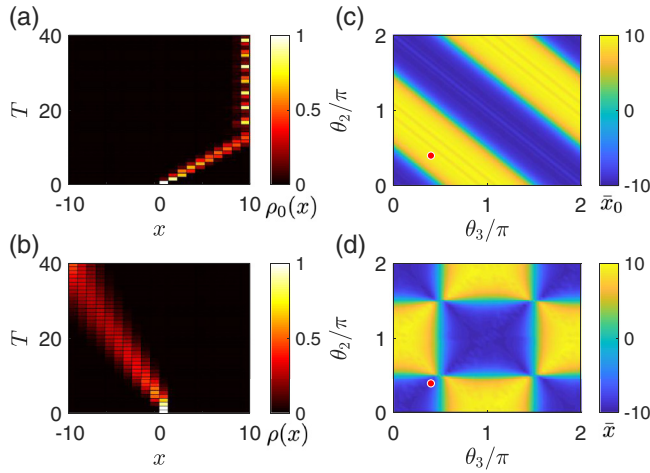
FIG. 3. (a),(b) Spatial distributions of the quantum walks for an initial state prepared in the middle of the system, governed by U_0 and U, the two quantum walks without and with the interchain hopping, respectively. (c),(d) Average position of the final for the two quantum walks at $T = 40$ versus the two angles θ_2 and θ_3. Yellow and blue (bright and dark) regimes indicate nonreciprocal pumping toward the directions of $x = N$ and $x = -N$, respectively. The red points in (c),(d) represent the two cases of (a),(c), with $\theta_2 = \theta_3 = 0.4\pi$. Other parameters are $\alpha_a = \alpha_b = 3$, $\theta_1 = 0.2\pi$, and $N = 10$.

same preferred walk direction, their coupling can reverse the direction of transport, thus demonstrating direction reversal of NHSE via time evolution dynamics.

We consider an initial state prepared in the middle of the system, $\Psi_{\text{ini}} = \frac{1}{\sqrt{2}}(|a, 0\rangle \otimes |\uparrow\rangle + |b, 0\rangle \otimes |\uparrow\rangle)$. In Figs. 3(a) and 3(b), we show the spatial distribution $\rho_0(x)$ of the normalized final state $\Psi_{0,\text{fin}} = U_0^T \Psi_{\text{ini}}$ and $\rho(x)$ of $\Psi_{\text{fin}} = U^T \Psi_{\text{ini}}$ for the quantum walk governed by U_0 and U, respectively. Here T represents the number of steps of the quantum walk and the normalized spatial distribution is defined as $\rho(x) = \sum_{s=a,b,\sigma=\uparrow,\downarrow} |\tilde{\psi}_{\text{fin}}^{x,s,\sigma}|^2$, with $\tilde{\psi}_{\text{fin}}^{x,s,\sigma}$ the wave amplitude of the normalized final state,

$$\tilde{\psi}_{\text{fin}}^{x,s,\sigma} = \frac{\psi_{\text{fin}}^{x,s,\sigma} |s, x\rangle \otimes |\sigma\rangle}{\sqrt{\sum_{x,s=a,b,\sigma=\uparrow,\downarrow} |\psi_{\text{fin}}^{x,s,\sigma}|^2}},$$

obtained from $\Psi_{\text{fin}} = \sum_{x,s=a,b,\sigma=\uparrow,\downarrow} \psi_{\text{fin}}^{x,s,\sigma} |s, x\rangle \otimes |\sigma\rangle$. It is clearly seen from Figs. 3(a) and 3(b) that introducing the interchain hopping reverses the propagation direction of the walker. In Figs. 3(c) and 3(d), we further examine the average position of the final state, defined as $\bar{x} = \sum_{x,s=a,b,\sigma=\uparrow,\downarrow} x |\psi_{\text{fin}}^{x,s,\sigma}|^2$. Note that this average is over both chains. Without the interchain hopping operators $S_{3,4}$, the quantum walk governed by U_0 exhibits the NHSE, of which the direction of nonreciprocal population accumulation is determined by the two rotation angles θ_1 and $\theta_2 + \theta_3$ in Eq. (9). As seen in Figs. 3(c) and 3(d), the interchain hopping can reverse the direction of particle transport. That is, when the color in Fig. 3(c) mismatches that in Fig. 3(d), reversed particle transport, as compared with the decoupled case, occurs. Combining the results in Figs. 3(c) and 3(d), we obtain the parameter regime in Fig. 4(a) on the $\theta_3 - \theta_2$ plane, where reversed particle transport is observed.
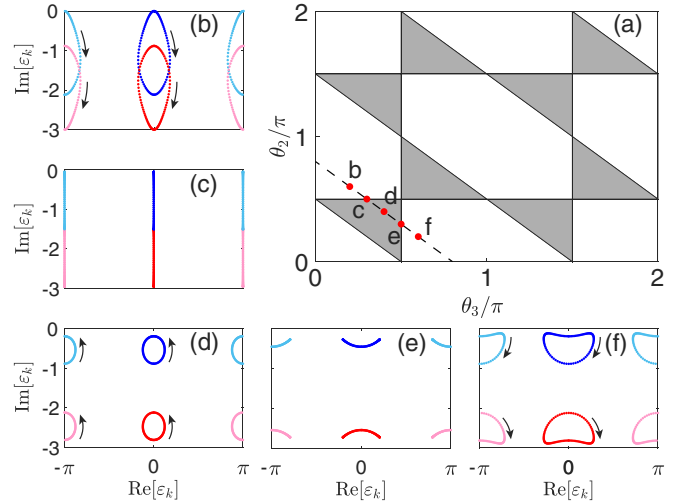

FIG. 4. (a) Phase diagram obtained from Figs. 3(c) and 3(d); reversed nonreciprocal accumulation occurs for the parameters falling in the gray areas. (b)–(f) The quasienergy spectra of U_k with different parameters, corresponding to the five red dots along the black dash line with $\theta_2 + \theta_3 = 0.8\pi$ in panel (a). Different colors mark the four bands of the spectra (blue, red, cyan, and pink). Black arrows indicate the winding direction of the quasienergies with k varying from 0 to 2π. The parameters are $\theta_2 = 0.2\pi, 0.3\pi, 0.4\pi, 0.5\pi$, and 0.6π from (b) to (f), with $\alpha_a = \alpha_b = 3$ and $\theta_1 = 0.2$ for all panels.

To further digest the direction reversal of NHSE, one may also investigate the winding behavior of the quasienergy ε_k, obtained from $U_k \Psi_k = e^{-i\varepsilon_k} \Psi_k$, with U_k being the Fourier transform of U, Ψ_k the eigenvectors of U_k, and k the Bloch momentum reflecting the translational invariance of the quantum walk model. The winding of the quasienergy spectrum as k increases from 0 to 2π is shown in Figs. 4(b) to 4(f). The direction of the winding is seen to change when the system parameters (θ_2, θ_3) move across the phase boundary identified in Fig. 4(a). There is hence a jump of the spectral winding number between ± 1 and 0, as we go from case (b) to case (f). In particular, as shown in Figs. 4(c) and 4(e), along the phase boundary, the quasispectrum in the k space does not enclose any area, corresponding to a trivial spectral winding and the absence of NHSE. These results further verify that the above observed reversal of particle transport direction is due to reversed NHSE.

To conclude, we note that particle transport with a reversed direction, as illustrated in Figs. 3(a) and 3(b), can be observed within very few quantum walk steps. The required lattice size can also be small since there is no need to distinguish between bulk sites and edge sites. In the Supplemental Material [72], we even add an example where reversed NHSE in our quantum walk system can be observed using only two unit cells.

Summary. We have shown that a coherent coupling between two 1D non-Hermitian chains can lead to direction reversal of NHSE for all the eigenmodes. This concept is demonstrated using both the spatial profile of stationary solutions, as well as time evolution dynamics on a quantum walk platform within reach of current experiments. In our first model, the common and individual direction of NHSE

is obvious, as observed from the nonreciprocal hopping on the two individual chains, yet a coupling between them yields a population accumulation along the reversed direction for every eigenmode of the system. This intriguing phenomenon is interpreted in terms of the interference between multiple hopping pathways and explained quantitatively via an adiabatic/hybridized representation. The simplicity of this two-chain model and the clear physics behind the anomalous direction reversal of NHSE indicate the general relevance of our findings in various non-Hermitian systems realizing the NHSE. One example is given by our second working model aiming at an experimental proposal to observe reversed NHSE on the dynamics level, where two individual chains hosting a quantum walker have the same preferred direction of particle transport, yet an interchain hopping can again reverse the direction of particle transport. In both models,

we have witnessed how a physical phenomenon analogous to ANM may emerge in contexts or experimental platforms of non-Hermitian physics. Our findings should also offer useful schemes to manipulate the NHSE by tuning the coherent coupling between individual subsystems. It should be stimulating to extend our findings to higher dimensions, where NHSE becomes a rather universal property of non-Hermitian systems, with the boundary localization behavior of bulk eigenmodes strongly dependent on the system's geometry [76].

[1] C. M. Bender and S. Boettcher, Real Spectra in Non-Hermitian Hamiltonians Having *PT* Symmetry, Phys. Rev. Lett. **80**, 5243 (1998).

[2] C. M. Bender, Making sense of non-Hermitian Hamiltonians, Rep. Prog. Phys. **70**, 947 (2007).

[3] I. Rotter, A non-Hermitian Hamilton operator and the physics of open quantum systems, J. Phys. A: Math. Theor. **42**, 153001 (2009).

[4] Y. Ashida, Z. Gong, and M. Ueda, Non-Hermitian physics, Adv. Phys. **69**, 249 (2020).

[5] E. J. Bergholtz, J. C. Budich, and F. K. Kunst, Exceptional topology of non-Hermitian systems, Rev. Mod. Phys. **93**, 015005 (2021).

[6] V. M. Martinez Alvarez, J. E. Barrios Vargas, and L. E. F. Foa Torres, Non-Hermitian robust edge states in one dimension: Anomalous localization and eigenspace condensation at exceptional points, Phys. Rev. B **97**, 121401(R) (2018).

[7] S. Yao and Z. Wang, Edge States and Topological Invariants of Non-Hermitian Systems, Phys. Rev. Lett. **121**, 086803 (2018).

[8] S. Yao, F. Song, and Z. Wang, Non-Hermitian Chern Bands, Phys. Rev. Lett. **121**, 136802 (2018).

[9] K. Yokomizo and S. Murakami, Non-Bloch Band Theory of Non-Hermitian Systems, Phys. Rev. Lett. **123**, 066404 (2019).

[10] C. H. Lee and R. Thomale, Anatomy of skin modes and topology in non-Hermitian systems, Phys. Rev. B **99**, 201103(R) (2019).

[11] F. Song, S. Yao, and Z. Wang, Non-Hermitian Skin Effect and Chiral Damping in Open Quantum Systems, Phys. Rev. Lett. **123**, 170401 (2019).

[12] D. S. Borgnia, A. J. Kruchkov, and R.-J. Slager, Non-Hermitian Boundary Modes and Topology, Phys. Rev. Lett. **124**, 056802 (2020).

[13] N. Okuma, K. Kawabata, K. Shiozaki, and M. Sato, Topological Origin of Non-Hermitian Skin Effects, Phys. Rev. Lett. **124**, 086801 (2020).

[14] K. Zhang, Z. Yang, and C. Fang, Correspondence between Winding Numbers and Skin Modes in Non-Hermitian Systems, Phys. Rev. Lett. **125**, 126402 (2020).

[15] C. H. Lee, L. Li, and J. Gong, Hybrid Higher-Order Skin-Topological Modes in Nonreciprocal Systems, Phys. Rev. Lett. **123**, 016805 (2019).

[16] L. Li, C. H. Lee, and J. Gong, Topological Switch for Non-Hermitian Skin Effect in Cold-Atom Systems with Loss, Phys. Rev. Lett. **124**, 250402 (2020).

[17] L. Li, C. H. Lee, S. Mu, and J. Gong, Critical non-Hermitian skin effect, Nat. Commun. **11**, 5491 (2020).

[18] J. C. Budich and E. J. Bergholtz, Non-Hermitian Topological Sensors, Phys. Rev. Lett. **125**, 180403 (2020).

[19] Y. Yi and Z. Yang, Non-Hermitian Skin Modes Induced by On-Site Dissipations and Chiral Tunneling Effect, Phys. Rev. Lett. **125**, 186802 (2020).

[20] L. Li and C. H. Lee, Non-Hermitian pseudo-gaps, Sci. Bull. **67**, 685 (2022).

[21] T. E. Lee, Anomalous Edge State in a Non-Hermitian Lattice, Phys. Rev. Lett. **116**, 133903 (2016).

[22] Y. Xiong, Why does bulk boundary correspondence fail in some non-Hermitian topological models, J. Phys. Commun. **2**, 035043 (2018).

[23] F. K. Kunst, E. Edvardsson, J. C. Budich, and E. J. Bergholtz, Biorthogonal Bulk-Boundary Correspondence in Non-Hermitian Systems, Phys. Rev. Lett. **121**, 026808 (2018).

[24] M. Lu, X.-X. Zhang, and M. Franz, Magnetic Suppression of Non-Hermitian Skin Effects, Phys. Rev. Lett. **127**, 256402 (2021).

[25] K. Deng and B. Flebus, Non-Hermitian skin effect in magnetic systems, Phys. Rev. B **105**, L180406 (2022).

[26] Y. Peng, J. Jie, D. Yu, and Y. Wang, Manipulating non-Hermitian skin effect via electric fields, arXiv:2201.10318v2.

[27] H. Jiang, L.-J. Lang, C. Yang, S.-L. Zhu, and S. Chen, Interplay of non-Hermitian skin effects and Anderson localization in nonreciprocal quasiperiodic lattices, Phys. Rev. B **100**, 054301 (2019).

[28] S. Longhi, Topological Phase Transition in non-Hermitian Quasicrystals, Phys. Rev. Lett. **122**, 237601 (2019).

[29] Q.-B. Zeng, Y.-B. Yang, and Y. Xu, Topological phases in non-Hermitian Aubry-André-Harper models, Phys. Rev. B **101**, 020201(R) (2020).

[30] L. Li, C. H. Lee, and J. Gong, Impurity induced scale-free localization, Commun. Phys. **4**, 1 (2021).

[31] C.-X. Guo, C.-H. Liu, X.-M. Zhao, Y. Liu, and S. Chen, Exact Solution of Non-Hermitian Systems with Generalized Boundary Conditions: Size-Dependent Boundary Effect and Fragility of the Skin Effect, Phys. Rev. Lett. **127**, 116801 (2021).

[32] Y. Liu, Y. Zeng, L. Li, and S. Chen, Exact solution of the single impurity problem in nonreciprocal lattices: Impurity-induced size-dependent non-Hermitian skin effect, Phys. Rev. B **104**, 085401 (2021).

[33] B. A. Bhargava, I. C. Fulga, J. van den Brink, and A. G. Moghaddam, Non-Hermitian skin effect of dislocations and its topological origin, Phys. Rev. B **104**, L241402 (2021).

[34] F. Schindler and A. Prem, Dislocation non-Hermitian skin effect, Phys. Rev. B **104**, L161106 (2021).

[35] X.-Q. Sun, P. Zhu, and T. L. Hughes, Geometric Response and Disclination-Induced Skin Effects in Non-Hermitian Systems, Phys. Rev. Lett. **127**, 066401 (2021).

[36] D. Zou, T. Chen, W. He, J. Bao, C. H. Lee, H. Sun, and X. Zhang, Observation of hybrid higher-order skin-topological effect in non-Hermitian topolectrical circuits, Nat. Commun. **12**, 7201 (2021).

[37] Y. Li, C. Liang, C. Wang, C. Lu, and Y.-C. Liu, Gain-Loss-Induced Hybrid Skin-Topological Effect, Phys. Rev. Lett. **128**, 223903 (2022).

[38] W. Zhu and J. Gong, Hybrid skin-topological modes without asymmetric couplings, Phys. Rev. B **106**, 035425 (2022).

[39] Z. Oztas and N. Candemir, Su-Schrieffer-Heeger model with imaginary gauge field, Phys. Lett. A **383**, 1821 (2019).

[40] W. Zhu, W. X. Teo, L. Li, and J. Gong, Delocalization of topological edge states, Phys. Rev. B **103**, 195414 (2021).

[41] J. Cheng, X. Zhang, M.-H. Lu, and Y.-F. Chen, Competition between band topology and non-Hermiticity, Phys. Rev. B **105**, 094103 (2022).

[42] C. C. Wanjura, M. Brunelli, and A. Nunnenkamp, Topological framework for directional amplification in driven-dissipative cavity arrays, Nat. Commun. **11**, 3149 (2020).

[43] C. C. Wanjura, M. Brunelli, and A. Nunnenkamp, Correspondence between Non-Hermitian Topology and Directional Amplification in the Presence of Disorder, Phys. Rev. Lett. **127**, 213601 (2021).

[44] L. Xiao, T. Deng, K. Wang, G. Zhu, Z. Wang, W. Yi, and P. Xue, Non-Hermitian bulk–boundary correspondence in quantum dynamics, Nat. Phys. **16**, 761 (2020).

[45] L. Xiao, T. Deng, K. Wang, Z. Wang, W. Yi, and P. Xue, Observation of Non-Bloch Parity-Time Symmetry and Exceptional Points, Phys. Rev. Lett. **126**, 230402 (2021).

[46] K. Wang, T. Li, L. Xiao, Y. Han, W. Yi, and P. Xue, Detecting Non-Bloch Topological Invariants in Quantum Dynamics, Phys. Rev. Lett. **127**, 270602 (2021).

[47] B. J. Keay, S. Zeuner, S. J. Allen, Jr., K. D. Maranowski, A. C. Gossard, U. Bhattacharya, and M. J. W. Rodwell, Dynamic Localization, Absolute Negative Conductance, and Stimulated, Multiphoton Emission in Sequential Resonant Tunneling Semiconductor Superlattices, Phys. Rev. Lett. **75**, 4102 (1995).

[48] E. H. Cannon, F. V. Kusmartsev, K. N. Alekseev, and D. K. Campbell, Absolute Negative Conductivity and Spontaneous Current Generation in Semiconductor Superlattices with Hot Electrons, Phys. Rev. Lett. **85**, 1302 (2000).

[49] R. Eichhorn, P. Reimann, and P. Hänggi, Brownian Motion Exhibiting Absolute Negative Mobility, Phys. Rev. Lett. **88**, 190601 (2002).

[50] R. Eichhorn, P. Reimann, and P. Hänggi, Paradoxical motion of a single Brownian particle: Absolute negative mobility, Phys. Rev. E **66**, 066132 (2002).

[51] L. Machura, M. Kostur, P. Talkner, J. Łuczka, and P. Hänggi, Absolute Negative Mobility Induced by Thermal Equilibrium Fluctuations, Phys. Rev. Lett. **98**, 040601 (2007).

[52] J. Nagel, D. Speer, T. Gaber, A. Sterck, R. Eichhorn, P. Reimann, K. Ilin, M. Siegel, D. Koelle, and R. Kleiner, Observation of Negative Absolute Resistance in a Josephson Junction, Phys. Rev. Lett. **100**, 217001 (2008).

[53] A. Ros, R. Eichhorn, J. Regtmeier, T. T. Duong, P. Reimann, and D. Anselmetti, Absolute negative particle mobility, Nature (London) **436**, 928 (2005).

[54] D. Reguera, A Luque, P. S. Burada, G. Schmid, J. M. Rubi, and P. Hänggi, Entropic Splitter for Particle Separation, Phys. Rev. Lett. **108**, 020604 (2012).

[55] A. Słapik, J. Łuczka, P. Hänggi, and J. Spiechowicz, Tunable Mass Separation via Negative Mobility, Phys. Rev. Lett. **122**, 070602 (2019).

[56] P. K. Ghosh, P. Hänggi, F. Marchesoni, and F. Nori, Giant negative mobility of Janus particles in a corrugated channel, Phys. Rev. E **89**, 062115 (2014).

[57] A. Sarracino, F. Cecconi, A. Puglisi, and A. Vulpiani, Nonlinear Response of Inertial Tracers in Steady Laminar Flows: Differential and Absolute Negative Mobility, Phys. Rev. Lett. **117**, 174501 (2016).

[58] J. Cividini, D. Mukamel, and H. A. Posch, Driven tracer with absolute negative mobility, J. Phys. A: Math. Theor. **51**, 085001 (2018).

[59] J. Wang, G. Casati, and G. Benenti, Inverse Currents in Hamiltonian Coupled Transport, Phys. Rev. Lett. **124**, 110607 (2020).

[60] S. Weidemann, M. Kremer, T. Helbig, T. Hofmann, A. Stegmaier, M. Greiter, R. Thomale, and A. Szameit, Topological funneling of light, Science **368**, 311 (2020).

[61] W.-T. Xue, M.-R. Li, Y.-M. Hu, F. Song, and Z. Wang, Simple formulas of directional amplification from non-Bloch band theory, Phys. Rev. B **103**, L241408 (2021).

[62] M. Brandenbourger, X. Locsin, E. Lerner, and C. Coulais, Non-reciprocal robotic metamaterials, Nat. Commun. **10**, 4608 (2019).

[63] T. Helbig, T. Hofmann, S. Imhof, M. Abdelghany, T. Kiessling, L. W. Molenkamp, C. H. Lee, A. Szameit, M. Greiter, and R. Thomale, Generalized bulk-boundary correspondence in non-Hermitian topolectrical circuits, Nat. Phys. **16**, 747 (2020).

[64] A. Ghatak, M. Brandenbourger, J. van Wezel, and C. Coulais, Observation of non-Hermitian topology and its bulk–edge correspondence in an active mechanical metamaterial, Proc. Natl. Acad. Sci. USA **117**, 29561 (2020).

[65] T. Hofmann, T. Helbig, F. Schindler, N. Salgo, M. Brzezińska, M. Greiter, T. Kiessling, D. Wolf, A. Vollhardt, A. Kabaši *et al.*, Reciprocal skin effect and its realization in a topolectrical circuit, Phys. Rev. Research **2**, 023265 (2020).

[66] L. Zhang, Y. Yang, Y. Ge, Y.-J. Guan, Q. Chen, Q. Yan, F. Chen, R. Xi, Y. Li, D. Jia *et al.*, Acoustic non-Hermitian skin effect from twisted winding topology, Nat. Commun. **12**, 6297 (2021).

[67] Q. Liang, D. Xie, Z. Dong, H. Li, H. Li, B. Gadway, W. Yi, and B. Yan, Observation of Non-Hermitian Skin Effect and

Topology in Ultracold Atoms, Phys. Rev. Lett. **129**, 070401 (2022).

[68] N. Hatano and D. R. Nelson, Localization Transitions in Non-Hermitian Quantum Mechanics, Phys. Rev. Lett. **77**, 570 (1996).

[69] H.-Q. Liang, M. Sen, J. Gong, and L. Li, Anomalous hybridization of spectral winding topology in quantized steady-state responses, Phys. Rev. B **105**, L241402 (2022).

[70] S. Mu, L. Zhou, L. Li, and J. Gong, Non-Hermitian pseudo mobility edge in a coupled chain system, Phys. Rev. B **105**, 205402 (2022).

[71] F. Song, S. Yao, and Z. Wang, Non-Hermitian Topological Invariants in Real Space, Phys. Rev. Lett. **123**, 246801 (2019).

[72] See Supplemental Material at http://link.aps.org/supplemental/10.1103/PhysRevB.106.085427 for (i) results with weak hopping disorder, (ii) perturbative GBZ solution for two coupled Hatano-Nelson chains, (iii) further results of several extensions of the two coupled Hatano-Nelson chains, (iv) details of the operators of the two-chain quantum walk, and (v) quantum walk in a system with two unit cells, which includes Refs. [7,9,13,14,63,73,74].

[73] L. Li, C. H. Lee, and J. Gong, Geometric characterization of non-Hermitian topological systems through the singularity ring in pseudospin vector space, Phys. Rev. B **100**, 075403 (2019).

[74] S. Imhof, C. Berger, F. Bayer, J. Brehm, L. Molenkamp, T. Kiessling, F. Schindler, C. H. Lee, M. Greiter, T. Neupert, and R. Thomale, Topolectrical-circuit realization of topological corner modes, Nat. Phys. **14**, 925 (2018)

[75] Y. Qi, C. Qiu, M. Xiao, H. He, M. Ke, and Z. Liu, Acoustic Realization of Quadrupole Topological Insulators, Phys. Rev. Lett. **124**, 206601 (2020).

[76] K. Zhang, Z. Yang, and C. Fang, Universal non-Hermitian skin effect in two and higher dimensions, Nat. Commun. **13**, 2496 (2022).